Thermal lattice Bhatnagar-Gross-Krook model without nonlinear deviations in macrodynamic equations

Y. Chen, H. Ohashi, and M. Akiyama
Department of Quantum Engineering and Systems Science, University of Tokyo, 7-3-1 Hongo, Bunkyo-ku, Tokyo 113, Japan
(Received 29 December 1993; revised manuscript received 2 May 1994)

We present a thermal lattice Bhatnager-Gross-Krook (BGK) model in D-dimensional space for the numerical simulation of fluid dynamics. This model uses a higher-order velocity expansion for Maxwellian-type equilibrium distribution. In the meantime, the lattice symmetry has been upgraded to ensure isotropy for the sixth-rank velocity-moment tensor. These manipulations lead to macroscopic equations without the nonlinear deviations, from which conventional thermal or nonthermal lattice BGK models suffered. We demonstrate the improvements by conducting classical Chapman-Enskog analysis and by the numerical calculation of the structure of the shock wave front and the decaying rate of the kinetic energy in the shear wave flow. Parameters in the velocity expansion are explicitly given for example models in one, two, and three dimensions. The transport coefficients of the modeled one-dimensional (1D) and 2D fluids are numerically measured as well.

PACS number(s): 47.11.+j, 51.10.+y, 47.40.Hg, 47.40.Nm

I. INTRODUCTION

Since the proposal of lattice gas automata (LGA) [1] for the simulation of fluid flow, much attention has been paid to the discrete kinetic theory. The governing equation in this theory is called as the lattice Boltzmann equation (LBE). The LBE describes the dynamics of particle motion in the LGA model under the molecular chaos approximation. Later this equation was explicitly solved in simulation, in place of the Boolean dynamic equation of the LGA model, and formed an alternative method [12] in the lattice hydrodynamic field. Although being a derivation of the LGA model, the LBE method became popular rapidly among the enthusiastic researchers because it is noise free and so flexible that most of the physics of the real fluid could be recovered. These advantages may well be observed from the lattice BGK model [2,3], which, by introducing the elegant Bhatnagar-Gross-Krook (BGK) collision operator [4] into the lattice Boltzmann equation, was the latest development of the LBE method. Today, main reasons that can be forwarded to persuade a fluid dynamic expert to adopt the LBE method or the lattice BGK model as an alternative tool for numerical simulation lie in threefolds: the simplicity of the algorithm, the ease of dealing with the complicated geometric boundaries, and the high level of parallelism in the implementation.

Recent topics about lattice BGK models are concerned with the nonlinear deviations in the compressible regime and models in which thermal effects are included.

The term in the macrodynamic equation, which causes nonlinear deviations, was first derived for the nonthermal lattice BGK model by Qian and Orszag [5]. This term appears to be an additional dissipative expression in the right-hand side (rhs) of the macroscopic momentum equation. The macrodynamics of the modeled nonthermal fluid is actually governed by

$$(\text{Navier-Stokes equation}) + \sigma\partial_\beta\partial_\gamma(\rho u_\alpha u_\beta u_\gamma)\,. \quad (1)$$

Here "Navier-Stokes equation" refers only to the momentum equation, while ρ, $\vec{u}$ are the density of the modeled fluid and the flow velocity. σ is the nonlinear response coefficient defined as $(\frac{1}{2}-\tau)$, where τ is the relaxation time of the BGK collision operator. As the ratio of this term to the linear viscous term in the usual Navier-Stokes equation is proportional to the square of the Mach number, the dynamics of the modeled fluid may deviate significantly from that of the real fluid when the flow enters into the compressible regime.

Pioneer work on a 2D thermal lattice BGK model was published in Ref. [6], where the hexongal lattice and the second order velocity (of the modeled fluid) expansion for the equilibrium distribution were employed. The conservation of mass, momentum and energy in the microworld, and the lattice symmetry ensuring isotropy for the fourth rank velocity (of the flying particle)-moment tensor suggest macroscopic equations which look like those of the real fluid, except for some hidden deviation terms resembling the additional one in Eq. (1).

The conventional thermal lattice BGK model is therefore not free from the aforementioned nonlinear deviations, because of the existence of deviation terms in the macrodynamic equations. We find that the deviation term in the macroscopic momentum equation for such a model is similar to the one for the nonthermal model, while deviation terms in the energy equation are derived [8] to be proportional to $\partial_\alpha\partial_\beta(\rho e u_\alpha u_\beta)$, $\partial_\alpha\partial_\beta(\rho u_\alpha u_\beta)$, ..., etc. As these expressions are composed of higher-order terms, we infer that the higher-order velocity expansion (fourth), beyond that for the standard hydrodynamic phenomena, has to be considered for the equilibrium distribution if the effects of the nonlinear deviations are to be eliminated. In the meantime, the lattice should be symmetric enough to ensure isotropy up to the sixth-rank velocity-moment tensor so that terms

in the higher-order expansion of the equilibrium distribution can be correctly formalized into the macroscopic flux tensors. This symmetry cannot be realized on lattices consisting of regular polygons (such as the hexongal lattice), as they ensure tensors to be isotropic only up to the fourth rank. These arguments become more obvious in Sec. II B, where the discrete integrations of the velocity moments for the equilibrium distribution are calculated.

A model which is able to eliminate the nonlinear deviations shall be introduced below. We present the theoretical works concerning the microdynamics and macrodynamics in Sec. II. In Sec. III the transport coefficients of some modeled fluids will be numerically measured and the elimination of the nonlinear deviations will be illustrated in one and two dimensions. Section IV gives the concluding remarks.

II. LATTICE HYDRODYNAMICS

A. Lattice geometry and symmetry

As in the previous models [3,7], the lattice we employed is composed of several sublattices in D dimensions. The coordinate of base vectors of these sublattices may be represented by $k(\pm 1,\ldots,\pm 1,0,\ldots,0)$ and its permutations. The number of nonzero components is denoted as p, which also stands for the moduli of unit base vectors, and k is a multiplier for these moduli. Hence, the vector of lattice link, which would be taken as the velocity vector of particle may be denoted as $\vec{c}_{pki}$, and its modulus may be defined as $c_{pk}=k\sqrt{p}$. Here pk gives the index of sublattice and i counts from the 1st to the b_pth vectors lying on each node of the pk sublattice. The nth rank velocity-moment tensor, defined as $T^{(n)}_{pk\alpha\ldots\xi}=\sum_i c_{pki\alpha}\times\cdots\times c_{pki\xi}$, is crucial to the hydrodynamic derivation [1]. The odd rank tensors vanish naturally by the definition itself and in this model the second, fourth, and sixth rank tensors are required to be isotropic. It can be shown that, in D-dimensional space, these even rank tensors are generally written as

$$\begin{aligned}
T^{(2)}_{pk\alpha\beta} &= \vartheta_{pk}\delta_{\alpha\beta}\,, \qquad (2)\\
T^{(4)}_{pk\alpha\beta\gamma\delta} &= \psi_{pk}\Upsilon_{\alpha\beta\gamma\delta}\\
&\quad +\varphi_{pk}(\delta_{\alpha\beta}\delta_{\gamma\delta}+\delta_{\alpha\gamma}\delta_{\beta\delta}+\delta_{\alpha\delta}\delta_{\beta\gamma})\,,\\
T^{(6)}_{pk\alpha\beta\gamma\delta\zeta\xi} &= \Lambda_{pk}\Upsilon_{\alpha\beta\gamma\delta\zeta\xi}+\Omega_{pk}(\delta_{\alpha\beta}\Upsilon_{\gamma\delta\zeta\xi}+\cdots)\\
&\quad +\Theta_{pk}(\delta_{\alpha\beta}T^{(4)}_{pk\gamma\delta\zeta\xi}+\cdots)\,,
\end{aligned}$$

where δ is the Kronecker tensor and Υ is the higher-order version of such a tensor which equals unit if the indices are identical, or zero otherwise. The "..." inside the first parenthesis of $T^{(6)}_{pk\alpha\beta\gamma\delta\zeta\xi}$ represents terms with the permutation of the indices from α to ξ, and inside the second parenthesis from β to ξ. The specific values of ϑ_{pk}, ψ_{pk}, φ_{pk}, Λ_{pk}, Ω_{pk}, and Θ_{pk} could be obtained by calculating the products of the gauge vectors $(\pm\vec{c}_{p1i},\pm\vec{c}_{p1i}\pm\vec{c}_{p1j},\ldots,)$ and are listed in Table I for one-, two-, and three-dimensional spaces. In case $k\neq 1$, these values should be further multiplied by a factor k^n. With careful inspection of these parameters, we may infer that the anisotropic parts of flux tensors of various physical quantities, namely, $\sum_{pk}N_{pk}\psi_{pk}$, $\sum_{pk}N_{pk}\Lambda_{pk}$ and $\sum_{pk}N_{pk}\Omega_{pk}$, would vanish simultaneously if the particle densities on the different sublattices ($N_{pk}=\sum_i N_{pki}$) were properly tuned.

B. Lattice BGK equation and equilibrium distribution

The lattice BGK equation describes the dynamics of the particles, namely, the propagation and the collision occurring on the discrete spatial lattice, at discrete time steps and with discrete velocity sets. Taking the particle distribution on each lattice link as $N_{pki}(\vec{x},t)$, this equation appears to be

$$N_{pki}(\vec{x}+\vec{c}_{pki},t+1)-N_{pki}(\vec{x},t)=-\frac{1}{\tau}(N_{pki}-N^{[eq]}_{pki})\,. \qquad (3)$$

Here the collision of particles is replaced by a relaxation process through which the particle distribution is relaxed to its equilibrium value over a time period τ. In order to reproduce the Navier-Stokes fluid, the equilibrium distribution should be Maxwellian and depends only on the local conserved density of mass, momentum, and energy, which are defined by the following formulas,

$$\begin{aligned}
\rho &= \sum_{pki}N_{pki}\,, \qquad (4)\\
\rho u_\alpha &= \sum_{pki}N_{pki}c_{pki\alpha}\,,\\
\rho e &= \frac{1}{2}\sum_{pki}N_{pki}(c_{pki_\alpha}-u_\alpha)^2\,.
\end{aligned}$$

Here e is the density of thermal energy determined by

TABLE I. Numerical values of symmetric parameters appearing in the velocity-moment tensor for the basic sublattices in one, two, and three dimensions.

Dimensions	Symmetric parameters					
1D	$\vartheta_{11}=2$	$\psi_{11}=0$	$\varphi_{11}=\frac{2}{3}$	$\Lambda_{11}=0$	$\Omega_{11}=0$	$\Theta_{11}=\frac{2}{15}$
2D	$\vartheta_{11}=2$ $\vartheta_{21}=4$	$\psi_{11}=2$ $\psi_{21}=-8$	$\varphi_{11}=0$ $\varphi_{21}=4$	$\Lambda_{11}=2$ $\Lambda_{21}=-16$	$\Omega_{11}=0$ $\Omega_{21}=0$	$\Theta_{11}=0$ $\Theta_{21}=\frac{4}{3}$
3D	$\vartheta_{11}=2$ $\vartheta_{21}=8$ $\vartheta_{31}=8$	$\psi_{11}=2$ $\psi_{21}=-4$ $\psi_{31}=-16$	$\varphi_{11}=0$ $\varphi_{21}=4$ $\varphi_{31}=8$	$\Lambda_{11}=2$ $\Lambda_{21}=-52$ $\Lambda_{31}=128$	$\Omega_{11}=0$ $\Omega_{21}=4$ $\Omega_{31}=-16$	$\Theta_{11}=0$ $\Theta_{21}=8$ $\Theta_{31}=0$

the flight speed of particles. When the macroscopic flow speed is very much smaller than this speed, the local equilibrium distribution could be expanded, around the uniform equilibrium, into the Chapman-Enskog form with consideration for parity invariance of the regular lattices,

$$N_{pki}^{[eq]} = A_{pk} + M_{pk}(c_{pki\alpha}u_\alpha) + G_{pk}u^2 + J_{pk}(c_{pki\alpha}u_\alpha)^2 + Q_{pk}(c_{pki\alpha}u_\alpha)u^2 + H_{pk}(c_{pki\alpha}u_\alpha)^3 + R_{pk}(c_{pki\alpha}u_\alpha)^2u^2 + S_{pk}u^4 + \mathcal{O}(u^5)\,. \tag{5}$$

Parameters of the expansion depend only on the local ρ and e and could be written in this form,

$$X_{pk} = \rho\sum_{l=0}^{2} x_{pkl}e^l\,. \tag{6}$$

X_{pk} may represent any of $A_{pk}, M_{pk}, \ldots, S_{pk}$. Hence x_{pkl}'s are to be written as a_{pkl}, $m_{pkl}, \ldots$, etc. The specific values of these parameters can be determined by considering definitions for the densities of mass, momentum and thermal energy as well as lattice symmetric requirements for the higher-rank isotropy, and by matching the form of macroscopic equations with those of the real fluid. The specification of a lattice BGK model reduces to the specification of a set of parameters in the low speed expansion [like Eq. (5)] for the equilibrium distribution. We summarize the constraints to the parameters that would lead to the Navier-Stokes equations in Table II. Using these constraints and the expressions given in Eq. (2), the velocity moments of different orders for the equilibrium particle distribution are calculated in D dimensions as follows,

$$\sum_{pki} N_{pki}^{[eq]} = \rho\,, \tag{7a}$$

$$\sum_{pki} N_{pki}^{[eq]}c_{pki\alpha} = \rho u_\alpha\,, \tag{7b}$$

$$\sum_{pki} N_{pki}^{[eq]}c_{pki\alpha}c_{pki\beta} = \frac{2}{D}\rho e\delta_{\alpha\beta} + \rho u_\alpha u_\beta\,, \tag{7c}$$

$$\sum_{pki} N_{pki}^{[eq]}c_{pki\alpha}c_{pki\beta}c_{pki\gamma} = \rho u_\alpha u_\beta u_\gamma + \frac{2}{D}\rho e(u_\alpha\delta_{\beta\gamma} + u_\beta\delta_{\alpha\gamma} + u_\gamma\delta_{\alpha\beta})\,, \tag{7d}$$

$$\sum_{pki} N_{pki}^{[eq]}c_{pki\alpha}c_{pki}^2c_{pki\beta} = \frac{4(D+2)}{D^2}\rho e^2\delta_{\alpha\beta} + \frac{2}{D}\rho eu^2\delta_{\alpha\beta} + \frac{2(D+4)}{D}\times\rho eu_\alpha u_\beta + \rho u^2u_\alpha u_\beta\,. \tag{7e}$$

It is easily found that Eqs. (7a) and (7b) verify the definitions of the mass and momentum densities. Equation (7c) not only gives the Galilean invariant form of the momentum flux tensor on the Euler order but also verifies the definition of the density of thermal energy as well. It will be shown in Sec. II C that Equations (7d) and (7e) give rise to isotropic expressions for viscous dissipation and heat conduction in the macroscopic equations. Note that these results would be identical with those stated in Ref. [9], if they were reduced to the 3D case.

C. Macroscopic equations

The continuous macroscopic conservation relations of the lattice BGK model can be derived by using the multiscale technique [1,7]. First, the discrete lattice BGK equation [Eq. (3)] is Taylor-expanded, to the second order, into the continuous space and time form in the long wavelength and the low frequency limits. Next, the scaling of time and space, and the perturbation of particle distribution are written as follows:

$$\partial_t \mapsto \epsilon\partial_{t1} + \epsilon^2\partial_{t2}\,,\quad \partial_\alpha \mapsto \epsilon\partial_\alpha\,,\qquad N_{pki} = N_{pki}^{(0)} + \epsilon N_{pki}^{(1)}\,. \tag{8}$$

Here ϵ is a small quantity proportional to the Knudsen number. When these expressions are substituted into the expanded lattice BGK equation, terms on the first and second order of ϵ shall be picked up so that two continuous kinetic equations can be obtained. Macroscopic

TABLE II. Constraints to the parameters of the expanded $N_{pki}^{[eq]}$. Blanks mean no constraints. $Y_0, \ldots, Y_3$ are not constraints. They are used to calculate other parameters. For example, when j_{pk0} is known, Y_0 can be decided and used to calculate g_{pk0}, and so on.

	A_{pk}			M_{pk}		J_{pk}		G_{pk}		H_{pk}	Q_{pk}	R_{pk}	S_{pk}
	a_{pk0}	a_{pk1}	a_{pk2}	m_{pk0}	m_{pk1}	j_{pk0}	j_{pk1}	g_{pk0}	g_{pk1}	h_{pk0}	q_{pk0}	r_{pk0}	s_{pk0}
$\sum_{pk} b_p x_{pkl}$	1	0	0					$-\frac{Y_0}{D}$	$-\frac{Y_1}{D}$				$-\frac{Y_3}{D}$
$\sum_{pk} b_p c_{pk}^2 x_{pkl}$	0	2	0	D	0	Y_0	Y_1	$-\frac{D}{2}$	0		$-3DY_2$	Y_3	0
$\sum_{pk} \psi_{pk} x_{pkl}$	0	0	0	0	0	0	0	0	0	0	0	0	0
$\sum_{pk} \varphi_{pk} x_{pkl}$	0	0	$\frac{4}{D^2}$	0	$\frac{2}{D}$	$\frac{1}{2}$	0	0	$-\frac{1}{D}$	Y_2	$-\frac{1}{2}$	0	$-\frac{1}{2(D+2)}$
$\sum_{pk} \Lambda_{pk} x_{pkl}$						0	0			0		0	
$\sum_{pk} \Omega_{pk} x_{pkl}$						0	0			0		0	
$\sum_{pk} \Theta_{pk} x_{pkl}$						0	$\frac{1}{D}$			$\frac{1}{6}$		$\frac{1}{2(D+4)}$	

equations describing the conservation of mass, momentum and energy will emerge, if the velocity moments of different orders are taken and discrete integrations are carried out on these kinetic equations. Note that Eqs. (7a), (7b), and (7c) will ensure the macroscopic terms obtained from the first order equation to be physically correct. From Eqs. (7d) and (7e), we may have two more relations as follows:

$$\partial_{t1}\sum_{pki} N^{(0)}_{pki} c_{pki\alpha} c_{pki\beta} + \partial_\gamma \sum_{pki} N^{(0)}_{pki} c_{pki\alpha} c_{pki\beta} c_{pki\gamma} \quad (9)$$
$$= \frac{2}{D}\rho e \left[(\partial_\beta u_\alpha + \partial_\alpha u_\beta) - \frac{2}{D}\partial_\gamma u_\gamma \delta_{\alpha\beta} \right] ,$$

$$\partial_{t1}\sum_{pki} N^{(0)}_{pki} c_{pki\alpha} c^2_{pki} + \partial_\beta \sum_{pki} N^{(0)}_{pki} c_{pki\alpha} c^2_{pki} c_{pki\beta} \quad (10)$$
$$= \frac{4(D+2)}{D^2}\rho e \partial_\alpha e + \frac{2}{D}\rho e \left[(\partial_\beta u_\alpha + \partial_\alpha u_\beta) - \frac{2}{D}\partial_\gamma u_\gamma \delta_{\alpha\beta} \right] u_\beta .$$

These expressions are used to derive the correct constitutive relations, namely, the viscous stress and the heat flux, from the second order kinetic equation. Furthermore, the cancellation of terms on the second, the third, and the fourth order of u, terms which are related to the nonlinear deviations, is also realized. Terms for viscous works can be exactly generated. Note that the correct form of the viscous work would be ensured only for the models that employ the single time relaxation approximation, namely for the BGK models [13]. Finally, equations of two different orders are recombined, which gives rise to the following set of equations:

$$\partial_t \rho + \partial_\alpha(\rho u_\alpha) = 0 , \quad (11)$$

$$\partial_t(\rho u_\alpha) + \partial_\beta(\rho u_\alpha u_\beta) = -\partial_\alpha p + \partial_\beta \left[\mu(\partial_\alpha u_\beta + \partial_\beta u_\alpha) \right] + \partial_\alpha(\lambda \partial_\gamma u_\gamma) , \quad (12)$$

$$\partial_t(\rho e) + \partial_\alpha(\rho e u_\alpha) = -p\partial_\beta u_\beta + \partial_\alpha(\kappa' \partial_\alpha e) + \mu(\partial_\alpha u_\beta + \partial_\beta u_\alpha)\partial_\alpha u_\beta + \lambda(\partial_\beta u_\beta)^2 . \quad (13)$$

Here p is the thermodynamic pressure and is identified as this,

$$p = \frac{2}{D}\rho e . \quad (14)$$

μ and λ are the shear and the second viscosities, which are defined as in the following expressions:

$$\mu = \frac{2}{D}\rho e(\tau - \tfrac{1}{2}) , \quad (15)$$
$$\lambda = -\frac{4}{D^2}\rho e(\tau - \tfrac{1}{2}) .$$

Note that in the one-dimensional space, these viscous terms cancel each other and what we shall obtain is the Euler equation. On the other hand, bulk viscosity($\mu + \frac{2}{D}\lambda$) vanishes in the two-dimensional space so that the Navier-Stokes equations can be obtained if the shear viscosity is considered to be constant [10]. Heat conductivity may be identified provided that the temperature is properly defined. If the Boltzmann constant is set to have unit value, the temperature may be defined as $\frac{2}{D}e$, and this gives the heat conductivity as

$$\kappa = \frac{D}{2}\kappa' = \frac{D+2}{D}\rho e(\tau - \tfrac{1}{2}) . \quad (16)$$

The ratio of specific heats and the sound speed may be easily obtained as follows:

$$\gamma = \frac{D+2}{D} , \quad (17)$$

$$a_s = \sqrt{\frac{2(D+2)}{D^2}e} . \quad (18)$$

Although Eqs. (11), (12), and (13) have the same form as those published in Ref. [6], we emphasize that there are no hidden deviation terms in the r.h.s. any more. This shall be further demonstrated by the numerical calculations in the next section.

III. NUMERICAL RESULTS

We carried out all numerical calculations using the least one- and two-dimensional models. These models are denoted in the following sections as 1D5V and 2D16V, see the Appendix. To show the improvement achieved by the model, we also coded a 2D 13-velocity conventional lattice BGK model, in which the equilibrium distribution is expanded to the second order of u and the isotropy is kept only for the fourth-rank velocity-moment tensor. The numerical results are compared with each other in two cases.

We have to explain, before the results are shown, the unit system for these lattice gas models. As each particle, with a unit velocity vector, is propagated from one node to one of its nearest neighbors during one time step, we may define the metric unit as the distance between nodes, the spatial lattice spacing ℓ, and the temporal unit as the time interval for particle to fly from one node to another, the temporal lattice spacing $\triangle t$. The units of other thermodynamic variables and transport coefficients can be decided once the unit mass m for each particle is introduced. In the following presentation, all the units for various physical quantities will be omitted, while it is understood that they can be completely determined by using the aforementioned unit system based on the discrete spatial and temporal lattices.

A. Transport coefficients

We numerically measured sound speed, kinematic viscosity, and heat conductivity. The measured results are compared with the theoretical predictions made in Sec. II C. Figure 1 shows the results of sound speed, mea-

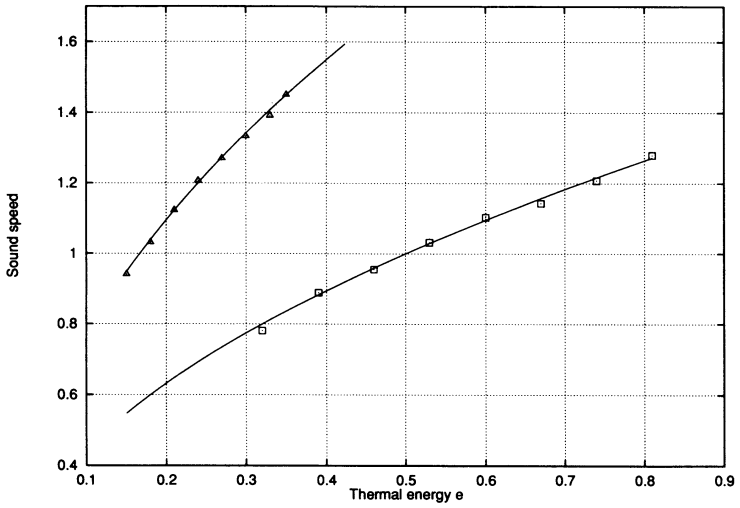

FIG. 1. Results of the numerical measurement of sound speed. Squares are the results of the 2D16V model, triangles are those of 1D5V, and solid lines are the results obtained from Eq. (18).

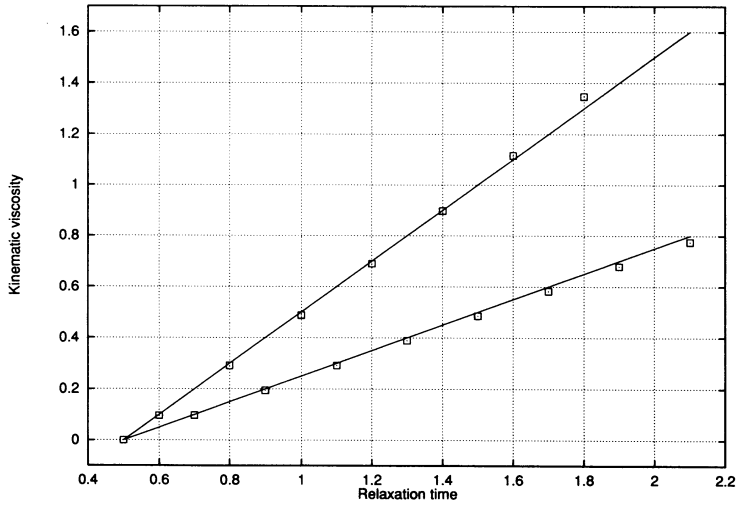

FIG. 2. Results of the numerical measurement of kinematic viscosity $\nu = \frac{\mu}{\rho_0}$. The measurement is carried out by simulating the relaxation of perturbations in the velocity field, under the condition $\rho_0 = 8.0$, $e_0 = 0.4$, and $e_0 = 0.8$. Solid lines are computed from Eq. (15) and squares are the measured results.

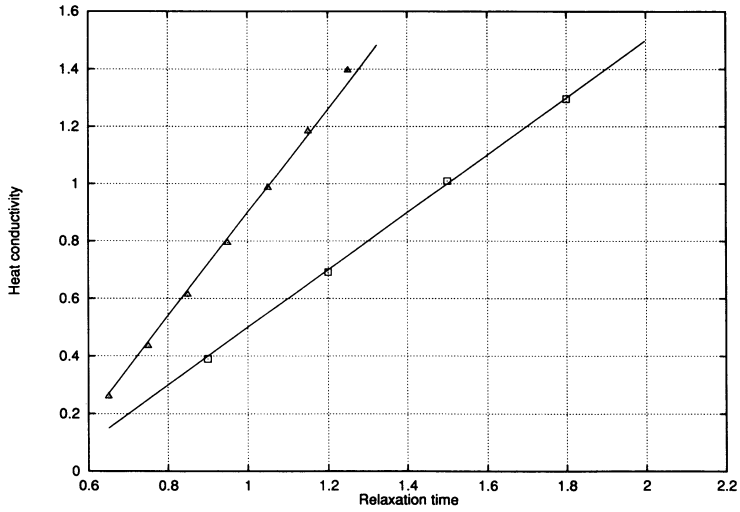

FIG. 3. Results of the numerical measurement of heat conductivity $\frac{\kappa'}{\rho_0}$. Again triangles are for the 1D model and squares are for the 2D model, while solid lines are computed by using Eq. (16). The measurement is carried out under the conditions $\rho_0 = 2.0$, $e_0 = 0.3$ for 1D5V and $\rho_0 = 8.0$, $e_0 = 0.5$ for 2D16V.

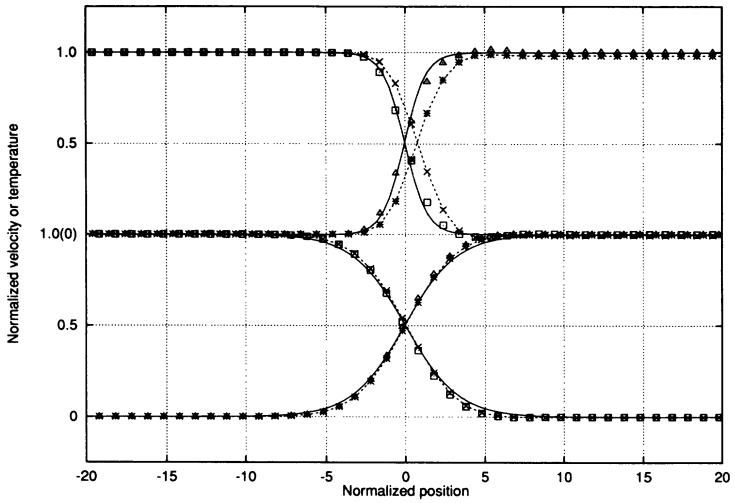

FIG. 4. Comparison of the structures of the shock wave fronts. Squares and triangles are the results of the 2D16V model, line points composed of dashed line and crosses or stars are results of the 2D13V model, and solid lines are the analytical solutions. The left-right step curve represents the sharp increase of temperature, while the right-left step curve stands for the increase of velocity. The upper half of the graph is for Ma=1.14 while the lower half is for Ma=1.02.

sured by employing the linear perturbation theory. The results of the 1D5V and 2D16V models agree well with the theoretical values. The measurement of the kinematic viscosity was only done for the 2D model and the results are shown in Fig. 2. We observed deviation from the theoretical value when τ got too large. This is due to the increment of the Knudsen number which may break the hydrodynamic mode. Heat conductivity was also measured for the 1D and 2D models. This was done by calculating the heat flux when the temperature gradient was kept constant. Both the models give satisfactory results, see Fig. 3.

B. Elimination of nonlinear deviations

The next two simulations are used to illustrate the effectiveness of the suggested model. Therefore, the results are compared with those obtained by using the conventional thermal lattice BGK model.

The first problem is the computation of the structure of the shock wave front. We simulated this 1D flow, however, by employing the 2D model on the 1000×1 lattices. In this case, the stagnation enthalpy $h + \frac{1}{2}u^2$ is constant [check Eqs. (13), (15), and (16)] throughout the wave, which should greatly simplify the procedure for the analytical solution [11]. Two runs of code were carried out under the conditions Ma=1.02 and 1.14, respectively. As shown in Fig. 4, the results of different models agree well with the analytical solution only when the Mach number is small enough. For the higher Mach number, the error of the conventional model is obviously larger.

We further illustrate the elimination of nonlinear deviations by simulating the shear wave flow

$$u_x = u_0, u_y = u_0 e^{i(\omega t + kx)}, \tag{19}$$

on a 64×64 lattice field. Here ω and k are the angular frequency and the wave number, respectively. The flow

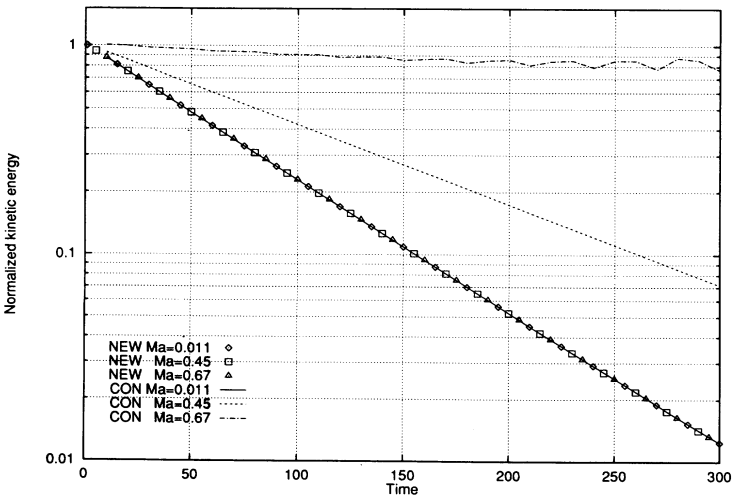

FIG. 5. Comparison of the Mach number effects on the decaying rate of the total kinetic energy in the shear wave flow. Different types of symbols are for the suggested model, while different types of lines are for the conventional model. The Mach numbers are set to be 0.011, 0.45, and 0.67 in three cases.

TABLE III. Parameters in the expanded equilibrium distribution function $N_{pki}^{[eq]}$ for the example one-, two-, and three-dimensional models. The first column gives the dimensions and the number of velocities in terms of "nDmV." The second column gives the indices of the sublattices and the numbers in the parentheses are the numbers of links on every node of those sublattices.

		A_{pk}			M_{pk}		G_{pk}		J_{pk}		Q_{pk}	H_{pk}	R_{pk}	S_{pk}
Model	Sublattice	a_{pk0}	a_{pk1}	a_{pk2}	m_{pk0}	m_{pk1}	g_{pk0}	g_{pk1}	j_{pk0}	j_{pk1}	q_{pk0}	h_{pk0}	r_{pk0}	s_{pk0}
1D5V	00(1)	1	$\frac{-5}{2}$	3	0	0	$\frac{-5}{4}$	3	0	0	0	0	0	$\frac{1}{4}$
1D5V	11(2)	0	$\frac{4}{3}$	-2	$\frac{2}{3}$	-1	$\frac{-1}{3}$	$\frac{1}{2}$	1	$\frac{-5}{2}$	$\frac{-17}{12}$	$\frac{5}{4}$	$\frac{-1}{4}$	$\frac{1}{12}$
1D5V	12(2)	0	$\frac{-1}{12}$	$\frac{1}{2}$	$\frac{-1}{24}$	$\frac{1}{4}$	$\frac{1}{48}$	$\frac{-1}{8}$	$\frac{-1}{64}$	$\frac{5}{32}$	$\frac{1}{24}$	0	$\frac{1}{64}$	$\frac{-1}{48}$
2D16V	11(4)	$\frac{8}{15}$	$\frac{-2}{3}$	$\frac{1}{3}$	$\frac{2}{3}$	-1	$\frac{-2}{3}$	$\frac{5}{6}$	$\frac{2}{3}$	-1	$\frac{-1}{2}$	$\frac{1}{3}$	$\frac{-1}{6}$	$\frac{1}{8}$
2D16V	12(4)	$\frac{-1}{30}$	$\frac{1}{24}$	$\frac{1}{24}$	$\frac{-1}{24}$	$\frac{1}{8}$	$\frac{1}{24}$	$\frac{-1}{12}$	$\frac{-1}{96}$	$\frac{1}{16}$	0	$\frac{1}{96}$	$\frac{1}{96}$	$\frac{-1}{64}$
2D16V	21(4)	$\frac{-4}{15}$	$\frac{2}{3}$	$\frac{-5}{12}$	0	$\frac{1}{4}$	$\frac{1}{6}$	$\frac{-7}{24}$	$\frac{1}{6}$	$\frac{-1}{8}$	$\frac{-1}{8}$	$\frac{1}{8}$	$\frac{-1}{48}$	$\frac{-1}{32}$
2D16V	22(4)	$\frac{1}{60}$	$\frac{-1}{24}$	$\frac{1}{24}$	0	0	$\frac{-1}{96}$	$\frac{1}{96}$	$\frac{-1}{384}$	$\frac{1}{128}$	0	0	$\frac{1}{768}$	0
3D40V	11(6)	$\frac{4}{15}$	$\frac{-29}{36}$	$\frac{8}{135}$	$\frac{2}{3}$	-1	$\frac{-1}{3}$	$\frac{-7}{32}$	$\frac{2}{3}$	$\frac{-1}{4}$	$\frac{1}{2}$	$\frac{1}{24}$	$\frac{-3}{56}$	$\frac{-177}{2240}$
3D40V	12(6)	$\frac{-1}{60}$	$\frac{-1}{36}$	$\frac{13}{540}$	$\frac{-1}{24}$	$\frac{1}{12}$	$\frac{1}{48}$	$\frac{-1}{24}$	$\frac{-1}{96}$	$\frac{1}{96}$	$\frac{-3}{64}$	$\frac{1}{384}$	$\frac{3}{448}$	$\frac{-1}{80}$
3D40V	21(12)	0	$\frac{5}{8}$	0	0	$\frac{1}{6}$	0	$\frac{53}{192}$	0	$\frac{1}{24}$	$\frac{-1}{8}$	$\frac{1}{48}$	$\frac{1}{112}$	$\frac{401}{4480}$
3D40V	31(8)	$\frac{-1}{15}$	$\frac{-5}{16}$	$\frac{-19}{270}$	0	0	0	$\frac{-23}{128}$	$\frac{1}{12}$	$\frac{-1}{32}$	0	$\frac{1}{192}$	$\frac{-3}{448}$	$\frac{-513}{8960}$
3D40V	32(8)	$\frac{1}{240}$	0	$\frac{17}{2160}$	0	0	0	0	$\frac{-1}{768}$	$\frac{1}{1536}$	0	0	$\frac{1}{7168}$	0

velocity u_0 can be changed to adjust the Mach number. The Mach number effects on the decaying rate of the total kinetic energy are investigated and shown in Fig. 5. We observed that the model behaved extremely well even if the Mach number reached 0.67. The decaying rates consistently stick to the value of $2\nu k^2$. For the conventional model, the deviation is intolerable even if the Mach number increases to the medium value of 0.45. However, this deviation agrees with the theoretically predicted nonlinear term [Eq. (1)] as well, for that the total kinetic energy decays as $e^{-2(\nu-\sigma u_0^2)k^2 t}$.

IV. CONCLUSION

We developed a thermal lattice BGK model which effectively eliminates the reported nonlinear deviations in the macrodynamic equations of the conventional models. This was demonstrated by both analytical derivation and numerical calculations. A detailed comparison between the results of the lattice BGK simulation of complicated flows and solutions of the Navier-Stokes equations obtained by those well-established numerical methods is very much expected and is under current research work.

APPENDIX: EXAMPLE MODELS

The specific forms of the expanded equilibrium distribution function $N_{pki}^{[eq]}$ are given in this appendix for one-, two-, and three-dimensional models. The parameters in the low speed expansion of the Maxwellian distribution [Eq. (5)] are obtained by solving the constraints listed in Table II. As some of these constraints are underconditioned, the solutions are somewhat arbitrary. All the example models are least ones, that is, the particle velocity sets are the smallest ones which could be employed to satisfy those constraints. In the one-dimensional space, four kinds of particles with different velocities and an additional rest particle are selected. The indices of the sublattices are 00 (for the stationary one), 11 and 12. In the two-dimensional space, sixteen types of particles flying on 11, 12, 21, and 22 sublattices are needed. In the three-dimensional space, however, forty types of particles, whose velocity vectors are identical with the link vectors of 11, 12, 21, 31, and 32 sublattices, have to be considered. One of the possible sets of parameters for the equilibrium distribution, for particles on different sublattices employed in different dimensional models, is listed in Table III.

[1] U. Frisch, B. Hasslacher, and Y. Pomeau, Phys. Rev. Lett. **56**, 1505 (1986).
[2] H. Chen, S. Chen, and W. Matthaeus, Phys. Rev. A **45**, 45 (1992).
[3] Y. H. Qian, D. d'Humières, and P. Lallemand, Europhys. Lett. **17**, 479 (1992).
[4] P. Bhatnagar, E. P. Gross, and M. K. Krook, Phys. Rev. **94**, 511 (1954).
[5] Y. H. Qian and S. A. Orszag, Europhys. Lett. **21**, 255 (1993).

[6] F. J. Alexander, S. Chen, and J. D. Sterling, Phys. Rev. E **47**, R2249 (1993).
[7] Y. Chen, H. Ohashi, and M. Akiyama (unpublished).
[8] Y. Chen, in Doctoral thesis, University of Tokyo, 1994.
[9] G. McNamara and B. Alder, Physica A **194**, 218 (1993).
[10] F. V. Hunt, in *AIP Handbook* (McGraw-Hill, New York, 1972).
[11] H. W. Liepmann, R. Narashimha, and M. T. Chahine, Phys. Fluids **5**, 1313 (1962).
[12] G. McNamara and G. Zanetti, Phys. Rev. Lett. **61**, 2332 (1988).
[13] G. McNamara (private communication).